Macromolecules
ARTICLE

Macromolecules **2010**, *43*, 6699–6705 **6699**
DOI: 10.1021/ma100917p

Soluble P3HT-Grafted Carbon Nanotubes: Synthesis and Photovoltaic Application

Biplab K. Kuila,[†] Kyusoon Park,[‡] and Liming Dai*[,§]

Department of Chemical and Materials Engineering, School of Engineering, University of Dayton, 300 College Park, Dayton, Ohio 45469. [†]Present address: Leibniz Institute of Polymer Research Dresden, 6 Hohe Strasse, Dresden 01069, Germany. [‡]Present address: Metal & Material Technology Group, R&D Center, LS Mtron Ltd. 555, Hogye-dong, Dongan-gu, Anyang-si, Gyeonggi-do, 431-080 South Korea. [§]Present address: Departments of Chemical Engineering and Macromolecular Science and Engineering, Case Western Reserve University, 10900 Euclid Avenue, Cleveland, OH 44106.

Received April 27, 2010; Revised Manuscript Received June 22, 2010

ABSTRACT: CH_2OH-terminated regioregular poly(3-hexylthiophene) (P3HT) was grafted onto carboxylic groups of acid-oxidized carbon nanotubes (CNTs) via esterification reaction. The P3HT-attached CNTs (P3CNTs) are soluble in common organic solvents, facilitating an intimate mixing with free P3HT chains for strong electronic interactions. The optical and electrochemical properties of the resultant nanocomposite were found to be different from the conventional composite, in which the pristine CNT and P3HT were physically mixed together (P3HT/CNT). Electrochemical measurements on the onset oxidation and reduction potentials of the P3CNT showed positive shifts by 0.06 and 0.1 eV, respectively, with respect to the corresponding values of pure P3HT, indicating that P3CNT has a lower highest occupied molecular orbital (HOMO) energy level and a lower lowest unoccupied molecular orbital (LUMO) energy level than those of pure P3HT. Bilayer photovoltaic devices with a thin film of pure P3CNT as the electron-donor and C_{60} as the electron-acceptor layer showed an increase in the power conversion efficiency by about 40% with respect to their counterpart based on pure P3HT.

Introduction

Conjugated polymers (CPs) with alternating C−C and C=C bonds have been extensively researched for several decades because of their enormous potential for a wide range of applications, including in sensors, energy storages, corrosion inhibitors, enzyme catalysts, and optoelectronic devices. Since the seminal paper on the first use of soluble regioregular poly(3-hexylthiophene) (P3HT) for semiconducting applications published in 1996,[1] regioregular P3HT has become one of the most widely studied CPs and the workhorse for polymeric transistors and photovoltaics due to its high optoelectronic performance and easy processability.[1−4] Optoelectronic properties of regioregular P3HT depend strongly on its molecular conformation and chain regioregularity.[5,6]

On the other hand, carbon nanotubes (CNTs), including multiwalled carbon nanotubes (MWNTs) and single-walled carbon nanotubes (SWNTs), have recently attracted considerable research interest due to its unique mechanical and electrical properties.[7−9] However, the potential application of CNTs is largely precluded by their poor proccessability. Therefore, many surface modification/functionalization methods have been developed to disperse CNTs in solutions and polymer matrice.[10] Of particular interest, composites of conjugated polymers and carbon nanotubes have been demonstrated to show certain synergetic effects arising from the good thermal-/photostability, high mechanical strength, and high electrical conductivity of carbon nanotubes as well as excellent optoelectronic properties of conjugated polymers.[11,12] For instance, the MWNT and poly(3-octylthiophene) (P3OT) composites prepared by physically mixing a hexane solution of MWNTs with a chloroform solution of P3OT showed an increase in the electrical conductivity by 5 orders of magnitude with respect to that of pure P3OT,[13] but the optical absorption spectra of their SWNT counterparts did not change significantly up to 5 wt % SWNT. This implies that there might be some physical interactions between the P3OT and CNTs whereas no significant ground-state electronic interaction took place between the two components to cause any significant charge transfer. Similar phenomena have been observed for P3HT and CNT composites.[11,14] Although the ground state interaction between the P3HT and carbon nanotubes in these nanocomposites is not sufficiently strong to produce any substantial change in the UV−vis spectra of P3HT,[11] photovoltaic cells based on the physically mixed P3HT and CNT nanocomposites showed enhanced device performance due to an improved P3HT crystallinity in the nanocomposite active layer. In the physically mixed composites, the CP and CNT interface is ill-defined and insufficiently intimated for an efficient charge transfer for optoelectronic applications. Although chemically functionalized CNTs have been used to achieve a homogeneous dispersion of carbon nanotubes in a polymer matrix,[15,16] it is still a challenge to ensure strong electronic interactions between the functionalized CNTs and free polymer chains in the matrix for efficient charge transfer/transport as the $\pi-\pi$ interaction alone has been shown to be insufficient to produce any significant ground-state electronic interaction.[11,13,14] In order to prepare CP and CNT nanocomposites with superb optoelectronic properties, we devised a chemical route to chemical attachment of P3HT chains directly onto CNTs (Schemes 1 and 2). Unlike conventional CP and CNT nanocomposites by physical mixing, the P3HT-grafted CNTs (i.e., P3CNTs) synthesized via Schemes 1 and 2 possess the most intimated connectivity between the two

*Corresponding author. E-mail: liming.dai@case.edu.

Published on Web 07/20/2010

Scheme 1. Reaction Scheme for the End-Functionalization of P3HT

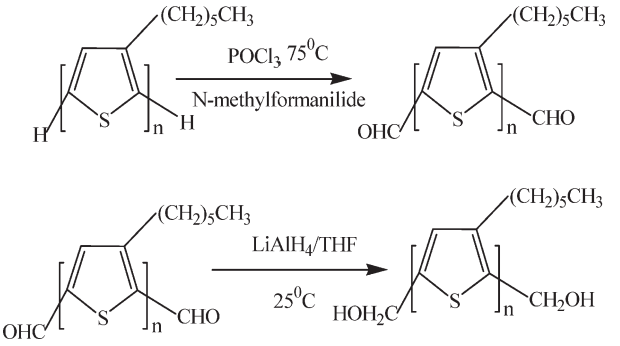

Scheme 2. Reaction Scheme for Grafting P3HT Chains onto Carbon Nanotubes

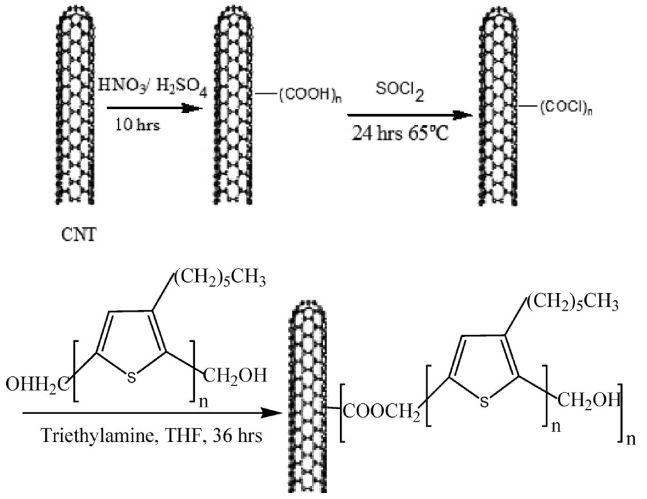

constituent components and hence strong electronic interactions. Herein, we report the synthesis and characterization of the newly developed P3CNTs for photovoltaic applications. To our best knowledge, the present study is the first case of soluble covalently bound P3HT-CNT to be used for enhancing the polymer solar cell performance.

Experimental Section

All chemicals, including regioregular P3HT ($M_w \sim 17\,500$, electronic grade, 99.995% metal basis), *N*-methylformanilide, toluene, $POCl_3$, triethylamine, $SOCl_2$, tetrabutylammonium hexafluorophosphate (Bu_4NPF_6), and acetonitrile, were purchased from Aldrich Chemicals and used as received. THF was obtained from Fischer Scientific and used immediately after distillation over Na wires.

The commercially available MWNTs, synthesized by pyrolysis of propylene using iron-based catalyst according to the published method[17] were purchased from Tsinghua and Nanfeng Chemical Group Cooperation, China, and were used after the acid purification.[18] Briefly, 300 mg of the pure MWNTs was suspended in 40 mL of concentrated sulfuric acid/nitric acid mixture (3:1 (v/v)) and sonicated for 10 h with an ultrasonicator (VWR model 75D), followed by repeated centrifugation and water washing to remove the acid residues. The resulting black solid was washed thoroughly with deionized water until the pH value reaches ~6. The purified MWNTs (Ox-MWNTs) were then dried at 60 °C in vacuum for overnight. The thermogravimetric analysis (TGA) of pristine carbon nanotube and the acid purified carbon nanotube are shown in Figure S1 (Supporting Information).

Functionalization of Regioregular P3HT with −CHO End Groups. Regioregular P3HT with −CHO end groups was prepared according to the reported method (Scheme 1).[19] Briefly, the commercially available P3HT (0.3 g) was dissolved in anhydrous toluene (80 mL) under nitrogen. Thereafter, *N*-methylformanilide (2 mL, 0.016 mol) and $POCl_3$ (1.3 mL, 0.014 mol) were added to the P3HT solution in toluene and kept at 75 °C for 24 h. The reaction mixture was then cooled to room temperature, followed by the addition of saturated aqueous solution of sodium acetate (20 mL) under stirring for another 2 h. The functionalized polymer was purified by precipitating in methanol, followed by repeated filtration and washing with methanol. Finally, the end-functionalization was confirmed by NMR measurements (Figure S2). ^{1}H NMR ($CDCl_3$): 0.9 (t, J = 6.33 Hz, 170 H), 1.48−1.36 (m, 340H), 1.62 (m, 112 H), 2.79 (t, J = 7.63 Hz, 120H), 6.96 (s, 56H), 10.02−9.85 (2s, 2H totally).

Functionalization of Regioregular P3HT with −CH_2OH End Groups. Regioregular P3HT with −CHO end groups (0.28 g, 0.035 mmol) was dissolved in anhydrous THF (80 mL) under nitrogen. $LiAlH_4$ solution in THF (1 M, 1.0 mL) was then added. The mixture was kept stirring at room temperature for 40 min. Hydrochloric acid solution (1 M, 1 mL) was then added to quench the $LiAlH_4$ residues. The resultant end-functionalized polymer was purified by precipitating in methanol, followed by repeated filtration and washing with methanol. The conversion of CHO to CH_2OH (Scheme 1) was confirmed by NMR measurements (Figure S3). ^{1}H NMR ($CDCl_3$): 0.9 (t, J = 6.33 Hz, 225 H), 1.48−1.36 (m, 450 H), 1.62 (m, 150 H), 2.79 (t, J = 7.63 Hz, 150H), 4.9−4.55 (2d, 4H totally, J = 5.62), 6.96 (s, 75H).

Functionalization of Carbon Nanotubes with P3HT (P3CNT). Scheme 2 shows the chemical reactions used for functionalization of carbon nanotubes with P3HT chains. In a typical experiment, an acid-oxidized MWNT sample (25 mg) was refluxed in thionyl chloride (25 mL) for 24 h, followed by the removal of excess thionyl chloride under vacuum. CH_2OH-terminated P3HT (100 mg) in 30 mL of THF was then added through a syringe to the thionyl chloride-treated MWNTs under stirring, followed by addition of triethylamine (1 mL) under an Ar atmosphere. After sonication for 2 h, the reaction mixture was vigorously stirred for 36 h, leading to a dark suspension. Solid materials in the suspension were removed by centrifuging at 5000 rpm for 10 min, and the solvent in the clear solution thus obtained was partially removed by evaporation. It was further purified by precipitating in methanol, followed by filtration and washing thoroughly to remove the excess triethylamine. The final product was dried in vacuum oven for 24 h at 60 °C. The NMR spectrum of the resultant P3CNT is given in Figure S4. ^{1}H NMR ($CDCl_3$): 0.9 (t, J = 6.33 Hz, 3 H), 2.0−1.0 (m, 8H), 2.8 (t, J = 7.63 Hz, 2H), 6.97 (s, 1H).

Device Fabrication. Polymer photovoltaic cells were fabricated using ITO as an anode and Ca/Al as a cathode. In a typical experiment, poly(3,4-ethylenedioxythiophene):poly(styrenesulfonate) (PEDOT:PSS) (Baytron P, ~30 nm thick) was spin-coated on an indium−tin oxide (ITO)-coated glass (~25 Ω/sq), which was precleaned sequentially with detergent (MICRO-90), deionized water, isopropyl alcohol, and acetone in an ultrasonic bath. A P3CNT thin film (70 nm) was then spin-coated from a chlorobenzene solution (10 mg/mL) on the PEDOT:PSS layer. After thermal annealing of the P3CNT film at 140 °C for 5 min, a thin layer of C_{60} (~45 nm) was vacuum ($< 10^{-6}$ Torr) evaporated onto the P3CNT surface as the electron acceptor. Subsequent vacuum (thermal) deposition of Ca (8 nm) and Al (130 nm) as the counter electrode completed the device fabrication. The effective area of the device is 6 mm^2. The thickness of films was measured using a Daktak 6 M surface profilometer. A solar simulator was used as the light source (AM1.5, 100 mW/cm^2), and the light intensity was monitored by a standard Si solar cell. Current−voltage ($I-V$) characteristics of the photovoltaic devices were measured with a computer-controlled Keithley 236 source measurement system. All the device manipulations and measurements were performed within a preparation glovebox under an Ar atmosphere. For comparison, bilayer photovoltaic cells

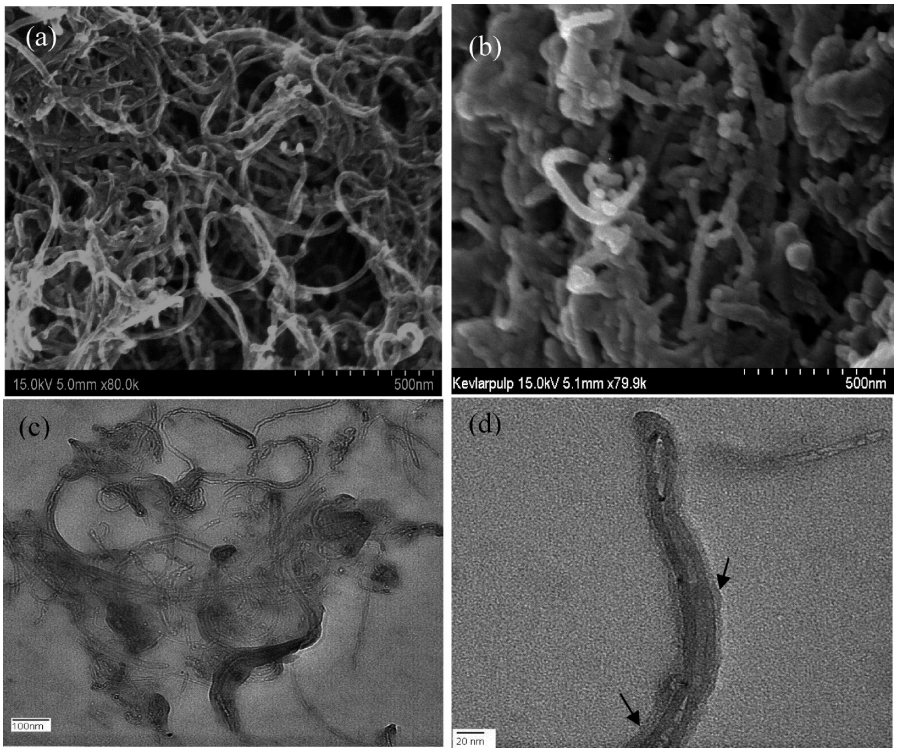

Figure 1. SEM images of (a) the acid purified MWNTs and (b) P3HT-grafted MWNTs (i.e., P3CNTs). TEM images of (c) P3CNTs and (d) as for (c) but under a higher magnification (the arrows point to the P3HT coating along the nanotube length.

based on pure P3HT/C_{60} and P3HT mixed with MWNTs (1%)/C_{60} were also fabricated and investigated under the same conditions.

Results and Discussion

As the cases for many other polymer-grafted carbon nanotubes,[12,20] the P3HT-grafted carbon nanotubes became highly soluble in various good solvents for P3HT, including chlorobenzene, THF, chloroform, and toluene. While the success in the CNT functionalization can be visualized from the solubility of the resultant P3CNTs in certain common solvents, the presence of a P3HT coating layer on the CNT surface was investigated by microscopic and spectroscopic measurements in this study.

Electron Microscopy. Parts a and b of Figure 1 show SEM images for the acid-purified carbon nanotubes (i.e., Ox-MWNTs) and the P3CNTs, respectively. As can be seen, Figure 1a shows a clean and smooth surface for the purified CNTs with an average diameter of ~20 nm, whereas Figure 1b reveals a distinctly different surface morphology with an apparently larger nanotube diameter due to the presence of the newly grated P3HT chains on the nanotube surface. Further evidence for the P3HT grafting came from TEM imaging. Figure 1c represents a typical TEM image for the P3CNT, which shows that the functionalized nanotubes are well-dispersed in the solvent (chloroform) used to prepare the TEM sample. The corresponding TEM image under a higher magnification shows a homogeneous polymer coating with a layer thickness of ~8 nm (Figure 1d).

X-ray Photoelectron Spectroscopy (XPS). XPS was used to monitor the end-functionalization shown in Scheme 2 and to determine the surface chemistry of P3CNTs. As expected, the XPS survey spectrum of P3HT given in Figure 2a shows peaks of carbon and sulfur only. While the XPS survey spectrum of the acid modified CNTs (Figure 2c) shows peaks for carbon and oxygen, the corresponding XPS spectrum for the P3CNT (Figure 2e) reveals peaks for carbon, sulfur, and oxygen, arising from the P3HT coating and the underlying carbon nanotubes. The high-resolution XPS C 1s spectrum of P3HT given in Figure 2b shows the expected hydrocarbon peak only. Figure 2d reproduces the high-resolution XPS C 1s spectrum for the acid-oxidized MWNTs, which shows the presence of O═C−OH (289 eV), C−O (286.2 eV), and C═C/C−C (~284.8 eV).[21−23] Figure 2f shows the high-resolution XPS C 1s spectrum for P3CNT. Compared with Figure 2d, Figure 2f shows a dramatic decrease in the peak component at 289 eV, indicating the occurrence of the reactions shown in Scheme 2. The peak components over 285−289 eV are still observable in Figure 2f, though not very well resolved due to the very low percentage of C−O and C═O bonds in the ester linkage in P3CNT. The numerical results from the XPS measurements are listed in Table 1. The similar C/S atomic ratios for P3HT and P3CNT indicate, once again, that the P3HT coating is homogeneous with a thickness close to the XPS detection depth (~10 nm).

Table 1. Percentage of the Surface Atoms and Their Atomic Ratios from XPS Measurements

	C 1s				
sample	C═O	C−O	C−H, C−C, C═C	C/O	C/S
P3HT			92.3		11.9
P3CNT	1.1	2.9	85.8	29.4	12.5
Ox-CNT	10	10	59	7.2	

TGA Analysis. The TGA thermograms of P3HT and the P3CNT are presented in Figure 3. As can be seen, P3HT and P3CNT exhibited a degradation temperature at 457.0 and 442.8 °C, respectively. The observed relatively low degradation temperature for P3CNT with respect to P3HT suggests that the former has a lower thermal stability than the latter. Unlike P3HT with no residues above 900 °C, however, P3CNT showed about 12% residual weight even at 1000 °C due to the presence of undegradable CNTs under a nitrogen atmosphere.[24,25] The above results indicate that the P3CNT contains

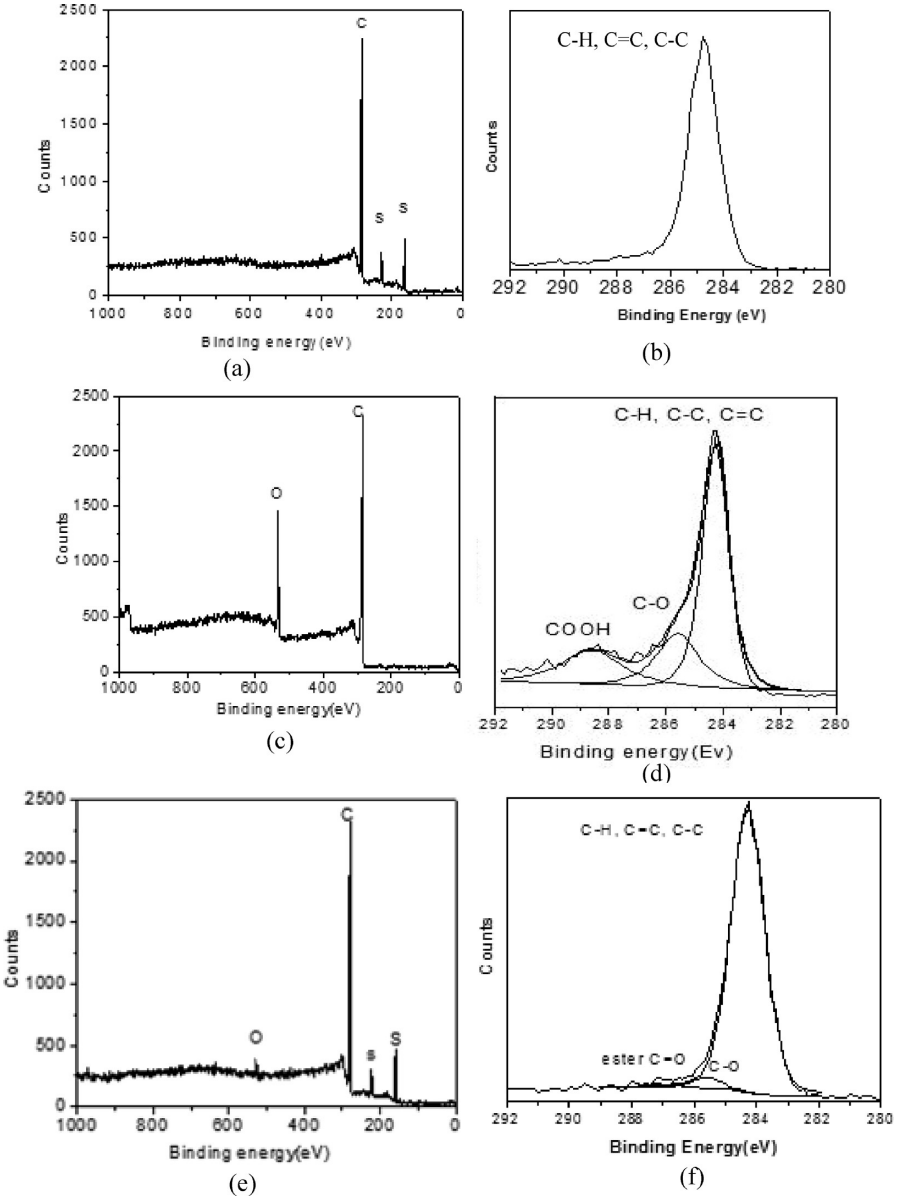

Figure 2. (a, c, e) XPS survey and (b, d, f) high-resolution of C 1s spectra of P3HT, Ox-MWNTs, and P3CNT, respectively.

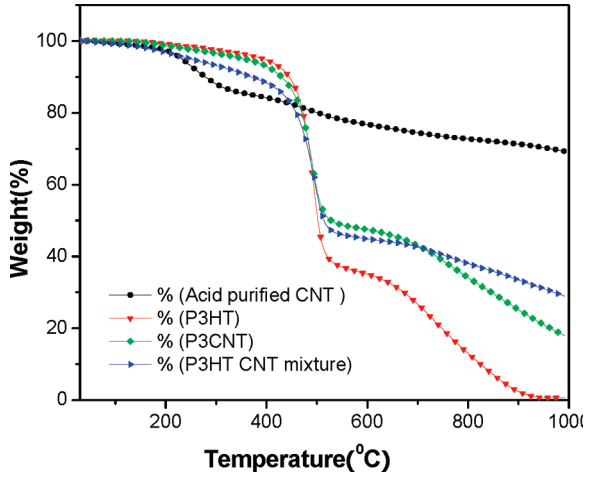

Figure 3. TGA thermogram of acid purified CNTs (i.e., Ox-MWNTs), P3HT, P3CNT, and P3HT/CNT mixture under a N_2 atmosphere at a heating rate of 20 °C/min.

at least about 12% CNTs. Now, the question arises why the thermal stability of P3CNT is lower than the pure P3HT. A similar decrease in the thermal stability of P3HT has been previously observed for P3HT and CNT nanocomposites.[24,26] In the present study, the observed decrease in thermal stability for P3CNT arises, most probably, from oxygen species associated with the ester linkage on the carbon nanotube surface that initiated the degradation of the covalently bonded P3HT chains. The chemical linkage between P3HT and carbon nanotube in the P3CNT was confirmed by further TGA measurements. As also shown in Figure 3, Ox-MWNTs show a gradual weight loss from about 30 to 400 °C due to thermal loss of water molecules absorbed by carboxyl acid groups on the nanotube surface. This gradual weight loss was also observed in Figure 3 for the P3HT and Ox-MWNT mixture but absent in P3CNT, indicating the disappearance of carboxyl acid groups from the CNT surface due to the formation of ester linkages between the P3HT chains and CNT surface in P3CNT.

DSC Thermogram. Figure 4a reproduced DSC thermograms of P3HT and P3CNT, which show melting points of

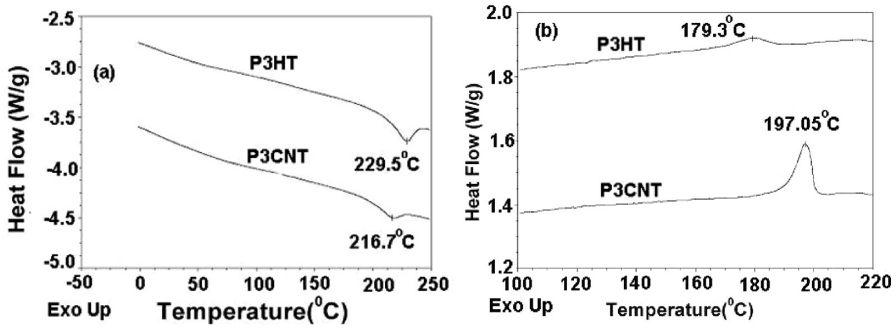

Figure 4. DSC thermograms of the P3HT and P3CNT: (a) heating and (b) cooling at a rate of 10 °C/min under a nitrogen atmosphere.

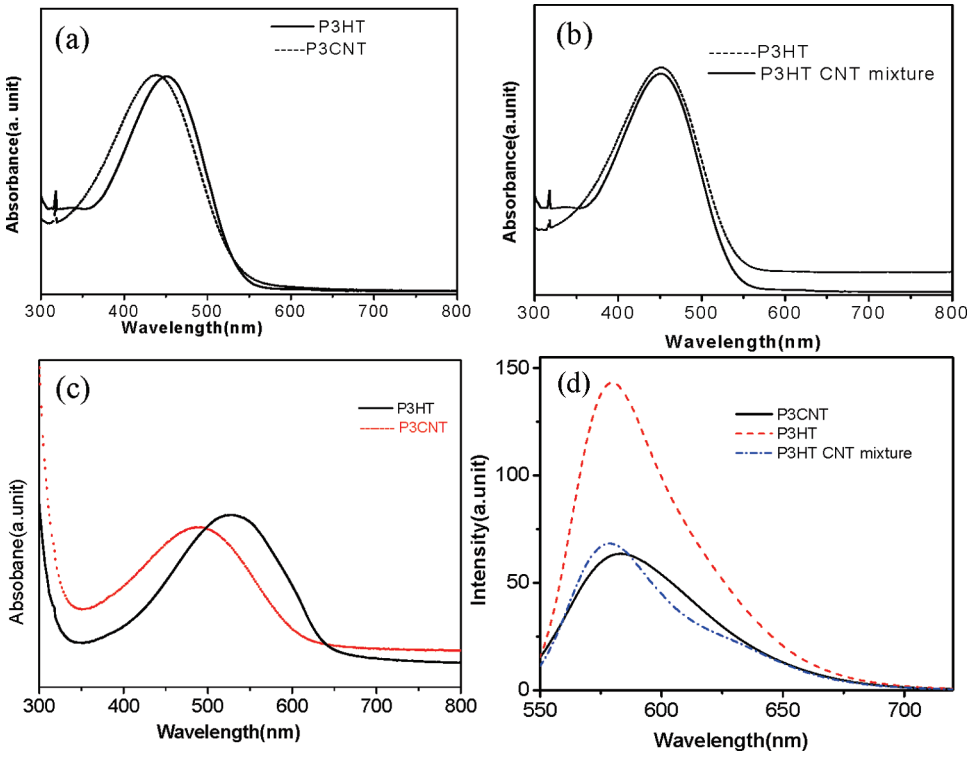

Figure 5. UV−vis absorption spectra of (a) P3HT and P3CNT, (b) P3HT and P3HT and CNT mixture in chloroform solution (0.0125 mg/mL) at 25 °C, (c) P3HT and P3CNT thin films spin-cast on glass substrates from chloroform solutions (10 mg/mL) at 25 °C. (d) Photoluminescence spectra of P3HT, P3CNT, and P3HT and CNT mixture in chloroform solution at 25 °C. The concentrations of all the sample solutions used for (d) are 1 mg/mL.

229.5 and 216.7 °C for P3HT and P3CNT, respectively, indicating a lower melting point for the CNT-grafted P3HT chains. The values of enthalpy of fusion (ΔH) for P3HT and P3CNT are 22.17 and 14.28 J/g, respectively. The decreased melting point and enthalpy of fusion observed for P3CNT indicate, most probably, a more amorphous structure for the P3HT chains grafted onto the curved CNT surface.[27] In order to investigate any possible nucleation effect of CNTs in enhancing the crystallization of P3HT chains, we also performed cooling measurements on the DSC instrument. Figure 4b shows that P3CNT started melt crystallization at 179.3 °C, which is 18 °C lower than that of pure P3HT in this particular case. This indicates that carbon nanotubes indeed inhibited the crystallization of P3HT, leading to a more disordered structure for P3HT chains grafted on the CNT surface with a decreased melting point.

UV−vis Absorption and PL Emission. Figure 5a shows the UV−vis absorption spectra of P3HT and P3CNT in chloroform (0.0125 mg/mL). As can be seen, P3HT exhibited an absorption band at 450 nm arising from the $\pi-\pi^*$ transition, which blue-shifted to 438 nm upon grafting onto CNTs in P3CNT. The simple mixture of P3HT and CNTs in the same solvent did not cause any significant change in the P3HT absorption band (Figure 5b), as is the case with other conjugated polymer and CNT composite systems.[13] Figure 5c shows the UV−vis absorption spectra for thin films (~40 nm) of pure P3HT and P3CNT. As expected, the P3HT thin film showed a significant red shift of the $\pi-\pi^*$ absorption up to 528 nm from the corresponding solution absorption at 450 nm, most probably due to the strong interchain interaction in the regioregular P3HT thin film. The absorption band of the P3CNT film centered at 492 nm, 36 nm below that of the P3HT thin film, though it also red-shifted from the corresponding solution absorption at 438 nm. The possible effect of end-functional groups on the optical absorption was checked to be insignificant (Figure S5).

It is important to understand why the $\pi-\pi^*$ absorption peak of P3CNT shifted to a lower wavelength while the simple mixture of P3HT and CNT did not show any significant change in the absorption spectrum of P3HT. Many factors, including molecular weight of the polymer,[28] solvent,[29] HT regioregularity,[30a] and chain conformation of the polymer,[6]

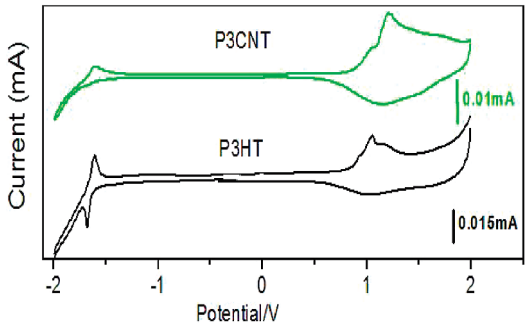

Figure 6. Cyclic voltammetry of the pristine P3HT and P3CNT films deposited on glassy carbon electrodes. Platinum was used as the counter electrode, silver wire as a reference electrode, and tetrabutylammonium hexafluorophosphate (Bu_4NPF_6) in acetonitrile as the supporting electrolyte.

are known to affect the optical absorption of P3HT. Since we used the highly regioregular P3HT sample of a well-defined molecular weight, the chain conformation effect could be dominate. P3HT chains grafted onto the curved CNT surface could have adopted more disordered chain conformation, leading to a less linear chain conformation in solution[29] and a more amorphous structure in the solid state (vide supra).

Figure 5d reproduced photoluminescence (PL) spectra for P3HT, P3CNT, and P3HT and CNT mixture in solution at an excitation wavelength of 450 nm, which shows PL emissions at about 579, 583, and 578 nm, respectively. While CNTs are well-known fluorescence quenchers,[30b] the photoluminescence quenching is more pronounced for P3CNT with respect to the physical mixture system of P3HT and CNTs (Figure 5d). This is an additional advantage for using the P3CNT in photovoltaic cells.

Electrochemistry. To demonstrate the potential application of the P3CNT in photovoltaic cells, we carried out cyclic voltammetry measurements of pure P3HT and P3CNT for determining their band gap energies (Figure 6). From the onset of oxidation (E_{ox}) and reduction (E_{red}) potentials observed in Figure 6, we can calculate the HOMO and LUMO energy levels as well as the energy gaps (E_g) of the polymers according to the following equations[31] with the units of E_{ox} and E_{red} in V vs Ag/Ag^+

$$\text{HOMO} = -e(E_{ox} + 4.4)\ \text{(eV)}$$

$$\text{LUMO} = -e(E_{red} + 4.4)\ \text{(eV)}$$

$$E_g = e(E_{ox} - E_{red})\ \text{(eV)}$$

The values of (E_{red} (V)/LUMO (eV), E_{ox} (V)/HOMO (eV)) for P3HT and P3CNT are (−1.4 V/−3.0 eV, 0.8 V/−5.2 eV) and (−1.3 V/−3.1 eV, 0.86 V/−5.26 eV), respectively. Thus, the band gap for P3CNT (2.16 eV) is slightly lower than that of pure P3HT (2.2 eV). Cyclic voltammetry study of CH_2OH end-functionalized P3HT and pure P3HT (Figure S6) showed no obvious difference in the electrochemical behavior. Therefore, the observed decrease in band gap for P3CNT arises from the direct interaction of the chemically grafted P3HT chains with high density of π-electrons presented at the carbon nanotube surface[32] to facilitate electron delocalization. As can be seen in Scheme 2, one end of the P3HT chain in the P3CNT will be grafted onto one carbon nanotube, while the other end of the same polymer chain may attach to the same or another carbon nanotube to form a continuous network structure. This should also facilitate the charge transport in photovoltaic cells.

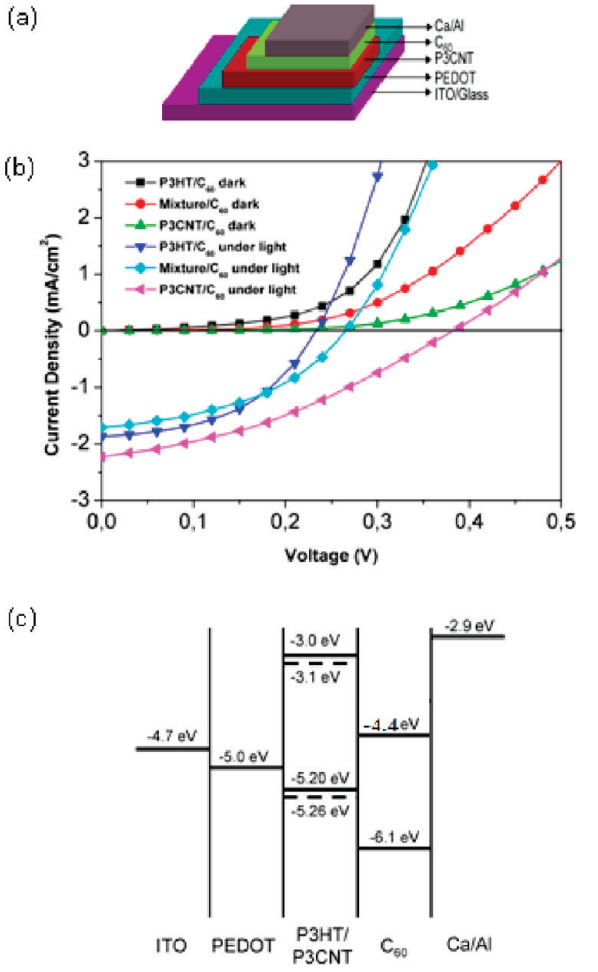

Figure 7. (a) Schematic diagram of the bilayer solar cell. (b) $I-V$ characteristics for photovoltaic cells based on the P3HT, mixture of P3HT and MWNTs (1%), and P3CNT under light illumination (AM1.5, 100 mW/cm^2). (c) Energy band diagram of an ITO/PEDOT/P3HT or P3CNT/Ca/Al bilayer devices (—, P3HT; ---, P3CNT).

Table 2. Device Parameters for Three Different Donor/C_{60} Bilayer Photovoltaic Cells

	V_{oc} (V)	I_{sc} (mA/cm^2)	FF	PCE (η) (%)
P3HT	0.23	1.9	0.48	0.21
P3HT and MWNTs (1%)	0.27	1.7	0.43	0.20
P3CNT	0.38	2.2	0.35	0.29

Photovoltaic Properties. As schematically shown in Figure 7a, polymer photovoltaic cells (PVs) with the structure of ITO/PEDOT:PSS (30 nm)/P3CNT or P3HT or mixture of P3HT and MWNTs (1%) (70 nm)/C_{60} (45 nm)/Ca (8 nm)/Al (130 nm) were fabricated. Figure 7b shows the current−voltage ($I-V$) curves for these PV devices, while Figure 7c gives the corresponding energy level diagrams.[34] The photovoltaic characteristics are listed in Table 2. Compared to PVs based on the pure P3HT or mixture of P3HT and CNTs, the P3CNT photovoltaic device shows an increased short circuit current (I_{sc}) and open circuit voltage (V_{oc}). V_{oc} is known to be determined by the energy difference between the LUMO of the C_{60} electron acceptor and HOMO of the electron donor in the bulk heterojunction solar cells.[33] The decrease in the energy level of HOMO for P3CNT with respect to P3HT seems also accountable for the increased V_{oc} observed for the bilayer photovoltaic cells based on the P3CNT, though its alone cannot cause such a significant increase. It was previously reported that nanotubes could act as the exciton

dissociation sites and/or hopping centers for hole transport.[35] Because of the intimated polymer−CNT contact in P3CNT, the PVs based on the P3CNT could possess higher capabilities for the exciton dissociation and charge carrier transport with respect to their P3HT counterparts, and hence about 40% increase in the power conversion efficiency (PCE). The relatively low fill factor for the P3CNT device (Table 2) indicates considerable room for further improvement in the device performance.

Conclusions

CH_2OH-terminated poly(3-hexylthiophene), P3HT, chains have been successfully grafted onto carboxylic groups of acid-oxidized carbon nanotubes, CNTs, via esterification reaction. The resultant P3HT-grafted carbon nanotubes (P3CNTs) are soluble in common organic solvents and compatible with pure P3HT chains, facilitating the structure/property characterization and device fabrication by solution processing. Although the P3CNT showed a blue shift in optical absorption with respect to P3HT in both solution and the solid state due to a less linear conformation for the CNT-bound polymer chains, our cyclic voltammetry measurements indicated a slightly lower band gap energy than that of P3HT for P3CNT because of the extensive electron delocalization between the chemically linked P3HT and CNT moieties in the P3CNT. Photovoltaic device based on P3CNT shows a higher short-circuit current and open-circuit voltage with an about 40% increase in power conversion efficiency than its counterparts based on pure P3HT or mixture of P3HT and MWNTs. Therefore, CNTs chemically grafted with conjugated polymers could be very useful hybrid materials for future optoelectronic applications.

Acknowledgment. L.D. thanks the support from AFOSR (FA9550-09-1-0331).

Supporting Information Available: Characterization details, supplementary figures for TGA (Figure S1), ^{1}H NMR spectra (Figures S2−S4), UV−vis spectrum (Figure S5), and cyclic voltammetry (Figure S6). This material is available free of charge via the Internet at http://pubs.acs.org.

References and Notes

(1) Bao, Z.; Dodabalapur, A.; Lovinger, A. J. *Appl. Phys. Lett.* **1996**, *69*, 4108.
(2) Bao, Z.; Lovinger, A. J. *Chem. Mater.* **1999**, *11*, 2607.
(3) Jeffries-El, M.; Sauve, G.; McCullough, R. D. *Macromolecules* **2005**, *38*, 10346.
(4) Coakley, K. M.; Liu, Y. X.; McGehee, M. D.; Findell, K. L.; Stucky, G. D. *Adv. Funct. Mater.* **2003**, *13*, 301.
(5) Schwartz, B. J. *Annu. Rev. Phys. Chem.* **2003**, *54*, 141.
(6) Lin, Y. H.; Jiang, C.; Xu, J.; Lin, Z. Q.; Tsukruk, V. V. *Soft Matter* **2007**, *3*, 432.
(7) Ajayan, P. M. *Chem. Rev.* **1999**, *99*, 1787.
(8) Baughman, R. H.; Zakhidov, A. A.; deHeer, W. A. *Science* **2002**, *297*, 787.
(9) Special Issue of Carbon Nanotubes. *Acc. Chem. Res.* **2002**, *35* (12).
(10) Tasis, D.; Tagmatarchis, N.; Bianco, A.; Prato, M. *Chem. Rev.* **2006**, *106*, 1105.
(11) Geng, J.; Zeng, T. *J. Am. Chem. Soc.* **2006**, *128*, 16827.
(12) Dai, L.; Mau, A. W.H. *Adv. Mater.* **2001**, *13*, 899.
(13) Musa, I.; Baxendale, M.; Amaratunga, G. A. J.; Eccleston, W. *Synth. Met.* **1999**, *102*, 1250.
(14) Pradhan, B.; Batabyal, S. K.; Pal, A. J. *J. Phys. Chem. B* **2006**, *110*, 8274.
(15) Tang, B. Z.; Xu, H. *Macromolecules* **1999**, *32*, 2569.
(16) O'Connell, M. J.; Boul, P.; Ericson, L. M.; Huffman, C.; Wang, Y. H.; Haroz, E.; Kuper, C.; Tour, J.; Ausman, K. D.; Smalley, R. E. *Chem. Phys. Lett.* **2001**, *342*, 265.
(17) Yu, H.; Zhang, Q.; Wei, F.; Qian, W.; Luo, G. *Carbon* **2003**, *41*, 2855.
(18) Zhu, L.; Chang, D. W.; Dai, L.; Hong, Y. *Nano Lett.* **2007**, *7*, 3592.
(19) Liu, J.; McCullough, R. D. *Macromolecules* **2002**, *35*, 9882.
(20) Hill, D. E.; Lin, Y.; Rao, A. M.; Allard, L. F.; Sun, Y. P. *Macromolecules* **2002**, *35*, 9466.
(21) Okpalugo, T. I. T.; Papakonstantinou, P.; Murphy, H.; McLaughlin, J.; Brown, N. M. D. *Carbon* **2005**, *43*, 153.
(22) Urszula, D. W.; Viera, S.; Ralf, G.; Sung, H. J.; Byung, H. K.; Hyun, J. L.; Lothar, L.; Yung, W. P.; Savas, B.; David, T.; Siegmar, R. *J. Am. Chem. Soc.* **2005**, *127*, 5125.
(23) Lee, W. H.; Kim, S. J.; Lee, W. J.; Lee, J. G.; Haddon, R. C.; Reucroft, P. J. *Appl. Surf. Sci.* **2001**, *181*, 121.
(24) Star, A.; Stoddart, J. F.; Steuerman, D.; Diehl, M.; Boukai, A.; Wong, E. W.; Yang, X.; Chung, S.-W.; Choi, H.; Heath, J. R. *Angew. Chem., Int. Ed.* **2001**, *40*, 1721.
(25) Kuila, B. K.; Malik, S.; Batabyal, S. K.; Nandi, A. K. *Macromolecules* **2007**, *40*, 278.
(26) Kuila, B. K.; Nandi, A. K. *J. Phys. Chem. B* **2006**, *110*, 1621.
(27) Prosa, T. J.; Winokur, M. J.; McCullough, R. D. *Macromolecules* **1996**, *29*, 3654.
(28) Trznadel, M.; Pron, A.; Zagorska, M.; Chrzaszcz, R.; Pielichowski, J. *Macromolecules* **1998**, *31*, 5051.
(29) Kobashi, M.; Takeuchi, H. *Macromolecules* **1998**, *31*, 7273.
(30) (a) Chen, T. A.; Wu, X.; Rieke, R. D. *J. Am. Chem. Soc.* **1995**, *117*, 233. (b) Chen, J.; Liu, H.; Weimer, W. A.; Halls, M. D.; Waldeck, D. H.; Walker, G. C. *J. Am. Chem. Soc.* **2002**, *124*, 9034.
(31) Sun, Q. J.; Wang, H. Q.; Yang, C. H.; Li, Y. F. *J. Mater. Chem.* **2003**, *13*, 800.
(32) Bavastrello, V.; Carrara, S.; Kumar, Ram, M.; Nicolini, C. *Langmuir* **2004**, *20*, 969.
(33) Scharber, M. C.; Mühlbacher, D.; Koppe, M.; Denk, P.; Waldauf, C.; Heeger, A. J.; Brabec, C. J. *Adv. Mater.* **2006**, *18*, 789.
(34) Meng, F.; Chen, K.; Tian, H.; Zuppiroli, L.; Nuesch, F. *Appl. Phys. Lett.* **2003**, *82*, 3788.
(35) Pradhan, B.; Batabyal, S. K.; Pai, A. J. *Appl. Phys. Lett.* **2006**, *88*, 093106.